IEEE Access
Multidisciplinary ⋮ Rapid Review ⋮ Open Access Journal

Received November 20, 2019, accepted December 29, 2019, date of publication January 13, 2020, date of current version January 22, 2020.

Digital Object Identifier 10.1109/ACCESS.2020.2966072

Anti-Multipath Orthogonal Chirp Division Multiplexing for Underwater Acoustic Communication

PEIBIN ZHU, XIAOMEI XU, XINGBIN TU, YOUGAN CHEN, (Senior Member, IEEE), AND YI TAO, (Member, IEEE)

Key Laboratory of Underwater Acoustic Communication and Marine Information Technology, Ministry of Education, Xiamen University, Xiamen 361005, China
College of Ocean and Earth Sciences, Xiamen University, Xiamen 361005, China

Corresponding author: Xiaomei Xu (xmxu@xmu.edu.cn)

This work was supported in part by the National Natural Science Foundation of China under Grant 41676024 and Grant 41976178.

ABSTRACT Multipath due to reflections of the sea surface, seabed, and obstacles, as well as inhomogeneity within the ocean, is an important characteristic of underwater acoustic channels. Mutual interference among multiple paths causes severe amplitude fading and frequency selective fading. The guard interval is an effective anti-multipath method, but an excessively long guard interval will reduce the data rate of multi-carrier underwater acoustic communication. In this paper, we propose a new anti-multipath multi-carrier communication method based on orthogonal chirp division multiplexing (OCDM) that uses chirp signals for carrier modulation. As OCDM exploits the multipath components for diversity gain, the system robustness is improved. The new method also adds a data pick-based rake receiver for maintaining good communication performance, even at short guard intervals. We detail the implementation and parameter selection of the anti-multipath OCDM system and compare its performance with the traditional orthogonal frequency division multiplexing (OFDM) scheme using simulations; under a severe multipath simulation condition (the delay spread is longer than the guard interval), the anti-multipath OCDM achieves a bit error rate (BER) of 10^{-6}, while the OFDM has a BER floor of 10^{-3}. The simulation results verify the feasibility of the proposed method and the superiority of its anti-multipath performance.

INDEX TERMS Multipath channels, orthogonal chirp division multiplexing, underwater acoustic communication.

I. INTRODUCTION

Research on underwater acoustic communication (UWAC) technology is important for both military and civilian applications. At present, UWAC is the core technology for underwater projects, such as ocean observation, coastal development, etc. These increasingly complex underwater projects necessitate higher requirements for UWAC; how to efficiently and reliably transmit the information through an underwater acoustic channel and further construct the UWAC network is the difficult point and hot spot in current UWAC research [1], [2]. Therefore, the design of the UWAC physical layer, based on the characteristics of the underwater acoustic channel, is essential. However, the underwater acoustic channel is an extremely complex and variable parametric random channel in time-space-frequency and is one of the most difficult wireless communication channels to master, especially in shallow waters [3], [4]. Non-coherent communication can provide better reliability. The representative chirp spread spectrum (CSS) modulation technique modulates symbols into a wider spectrum to obtain high processing gain but also sacrifices spectrum efficiency [5], so CSS technology is widely used in the application of reliable low-speed UWAC and telemetry remote control [6].

At present, high-speed UWAC systems employing single-carrier and multi-carrier modulation techniques have been widely examined. Many techniques have been studied to deal with the multipath delay and Doppler effect in underwater acoustic channels. For single-carrier communication, adaptive filter technology is very effective at eliminating inter-symbol interference (ISI), such as the application of a decision feedback equalizer with a recursive least squares

The associate editor coordinating the review of this manuscript and approving it for publication was Irfan Ahmed.

(RLS–DFE) algorithm [7], [8]. The channel tracker further eliminates the Doppler spread caused by the underwater acoustic channel [9], [10]. For multi-carrier communications, orthogonal frequency division multiplexing (OFDM) technology has been well studied in the past decades due to its high spectrum utilization and low receiver design complexity. The UWAC system based on OFDM technology is sensitive to Doppler shift and Doppler spread because the Doppler effect will destroy the orthogonality of the subcarriers. As a result, an inter-carrier interference (ICI) compensation algorithm [11] such as Doppler shift correction is usually required. In addition, larger Doppler spreads can be handled by the basis expansion model (BEM)-based signal design and channel coding techniques [12].

Recently, a new multi-carrier modulation system orthogonal chirp division multiplexing (OCDM) has been designed for optical fiber communication. Slightly different from traditional CSS technology, OCDM uses a set of orthogonal chirp signals for symbol modulation. Therefore, OCDM maximizes spectral efficiency while maintaining the robustness of CSS technology [13]. An underloaded OCDM scheme is proposed and leads to signal-to-noise ratio (SNR) gain but at the expense of the decreasing data rate [14]. Compared with the traditional OFDM system, the OCDM system offers better anti-interference ability while maintaining the same spectral efficiency [15]. However, the reflection of the sea surface, seabed, and obstacles, as well as inhomogeneity within the ocean, lead to multipath characteristics of the underwater acoustic channel, especially in shallow waters, that can reach tens or even hundreds of milliseconds [16]. Implementing a guard interval (GI) is an effective anti-multipath method, but an excessively long guard interval will reduce the data rate of multi-carrier UWAC. OCDM is sensitive to ICI caused by delay spread, especially in the shallow water environment with severe multipath. In this paper, we propose a new OCDM system, including a data pick-based rake receiver. We name it as Data Pick-Rake OCDM (DP-Rake OCDM). As the OCDM data block is analyzed through multiple time windows to find the best rake finger, the bit error rate (BER) of the system is reduced when the guard interval is short.

This paper is structured as follows: Section II describes the basic principles of OCDM and the data pick-based rake receiver. The channel models and the transmission scheme of the DP-Rake OCDM system are detailed in Section III. Section IV compares OCDM with traditional OFDM using simulations and discusses the results. Section V summarizes this article.

II. PRINCIPLE OF ANTI-MULTIPATH OCDM

A. OCDM BASICS

Similar to OFDM based on Fourier transform, OCDM is based on Fresnel transform. Fresnel transform is an important transformation derived from classical optics [17], and its core basis is the chirp signal. We can construct a set of mutually orthogonal chirp signals as the core basis of the OCDM system, represented by $\psi_n(t)$, that can be express as:

$$\psi_n(t) = e^{j\frac{\pi}{4}} e^{-j\pi \frac{N}{T^2}(t-n\frac{T}{N})^2}, \quad 0 \le t \le T \tag{1}$$

where n is the index of the chirp waveforms, N is the number of the chirp waveforms, and T is the duration of chirp waveforms. It can be easily proved in (2) that the set of chirp signals are mutually orthogonal:

$$\int_0^T \psi_m^*(t)\psi_k(t)dt = \int_0^T e^{j\pi \frac{N}{T^2}(t-m\frac{T}{N})^2} e^{-j\pi \frac{N}{T^2}(t-k\frac{T}{N})^2} dt = \delta(m-k) \tag{2}$$

In OFDM, linear exponential waveforms are chosen as the basis function. These exponential waveforms are orthogonal in the frequency domain, as shown in Fig. 1(a). For comparison, the orthogonal chirp waveforms of OCDM for $N = 16$ are shown in Fig. 1(b).

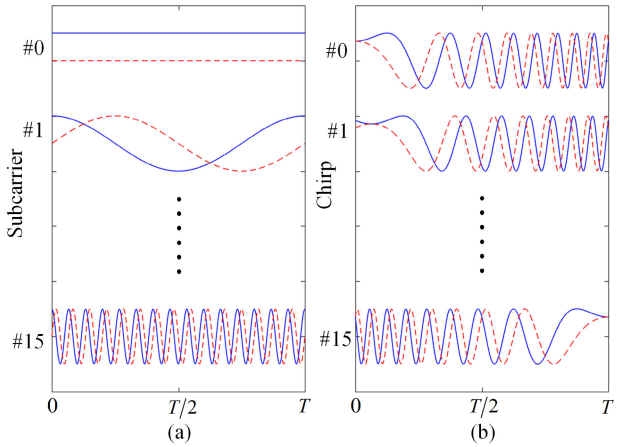

FIGURE 1. When $N = 16$, the in-phase (solid) and the quadrature (dotted) components of the (a) linear exponential waveforms in OFDM, and (b) chirped waveforms in OCDM.

In the OCDM system, both amplitude and phase information can be modulated in chirp waveforms. Modulation methods, such as PAM, PSK, and QAM, can be applied to the OCDM system. In a severe multipath underwater acoustic channel, the amplitude of the received waveform changes rapidly. Here, we choose QPSK as the modulation method. Denoting the kth symbol as $x(k)$ after QPSK mapping, the modulated signal $s(t)$ for OCDM is then expressed as:

$$s(t) = \sum_{k=0}^{N-1} x(k)\psi_k(t), \quad 0 \le t \le T \tag{3}$$

According to the orthogonality in (2), $x(m)$ can be easily extracted by the matched filter:

$$x'(m) = \int_0^T s(t)\psi_m^*(t)dt = \sum_{k=0}^{N-1} x(k)\delta(m-k) = x(m) \tag{4}$$

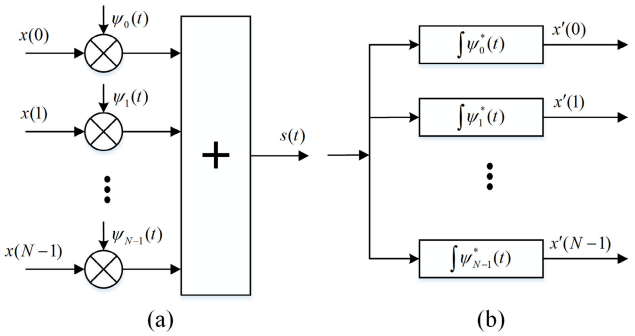

FIGURE 2. Schematic diagram of the OCDM system (a) multiplexing and (b) demultiplexing a bank of N modulated orthogonal chirp waveforms.

According to (3) and (4), the multiplexing at the transmitter and demultiplexing at the receiver in the OCDM system are shown in Fig. 2.

The basic processes of the analog OCDM system are expressed in (3) and (4), but they cannot be applied to the discrete-time signal in the current actual UWAC system. Therefore, the inverse discrete Fresnel transform (IDFnT) is often used in the digital OCDM system. $s(n)$ can be obtained by sampling the analog signal in (3) as:

$$\begin{aligned} s(n) &= F_{\psi}^{-1}\{x(k)\} \\ &= \begin{cases} \sum_{k=0}^{N-1} x(k)\psi_k(n\frac{T}{N}) & N \equiv 0(\mathrm{mod}2) \\ \sum_{k=0}^{N-1} x(k)\psi_k(n\frac{T}{N}+\frac{T}{2N}) & N \equiv 1(\mathrm{mod}2) \end{cases} \\ &= e^{j\frac{\pi}{4}} \sum_{k=0}^{N-1} x(k) \times \begin{cases} e^{-j\frac{\pi}{N}(n-k)^2} & N \equiv 0(\mathrm{mod}2) \\ e^{-j\frac{\pi}{N}(n-k+\frac{1}{2})^2} & N \equiv 1(\mathrm{mod}2) \end{cases} \end{aligned} \quad (5)$$

As in (5), the expression of IDFnT is slightly different when N is even or odd. In an actual OCDM UWAC system, N is usually selected as an even number to facilitate calculation. According to (5), OCDM modulation can be expressed as a compact matrix form, as follows:

$$\mathbf{s} = \mathbf{\Phi}^H \mathbf{x} \quad (6)$$

where $\mathbf{s} = [s(0), s(1), \ldots, s(N-1)]^T$ is the discrete-time domain signal after OCDM modulation, $\mathbf{x} = [x(0), x(1), \ldots, x(N-1)]^T$ is the symbol vector after mapping, and $\mathbf{\Phi}$ is discrete Fresnel transform (DFnT) matrix. For the case where N is even, the matrix $\mathbf{\Phi}$ can be expressed as:

$$\{\mathbf{\Phi}\}_{n,k} = \frac{1}{\sqrt{N}} e^{-j\frac{\pi}{4}} e^{j\frac{\pi}{N}(n-k)^2} \quad (7)$$

Since the DFnT matrix is a unitary matrix, at the receiver, the transmitted symbol can be recovered by the inverse operation DFnT of (6), as follows:

$$\mathbf{x}' = \mathbf{\Phi}\mathbf{s} = \mathbf{x} \quad (8)$$

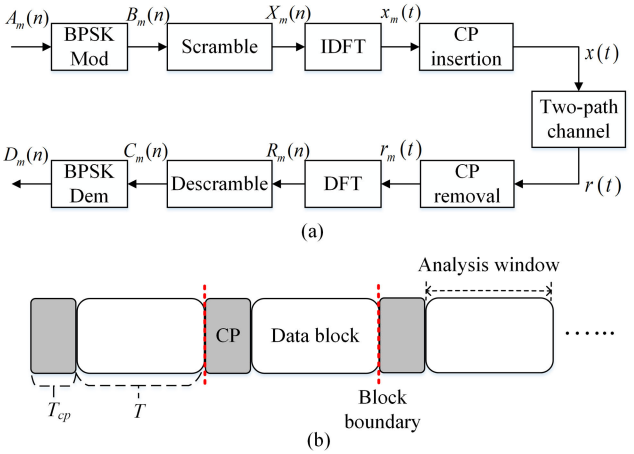

FIGURE 3. Basic model and frame structure. (a) Basic OFDM model and (b) frame structure and timing positions for the analysis window.

B. DATA PICK-BASED RAKE RECEIVER

In the multi-carrier UWAC demodulation process, communication performance will be deteriorated by multipath delay and Doppler spread. The effectiveness of Doppler compensation has been previously examined [18], and this paper focuses on the impact and elimination of multipath delay. This section describes a data pick-based rake receiver that is used to combat the effects of severe multipath effects at short guard intervals, thereby improving communication performance.

It is evident that severe multipath will introduce inter-block interference (IBI). IBI does not cause symbol errors at a high SNR. Generally, the SNR can be effectively improved by diversity technology. However, ICI caused by severe multipath is less obvious. To illustrate the principle of the data pick-based rake receiver and discuss it conveniently, we construct a familiar basic OFDM model, as shown in Fig. 3(a). At the transmitter, the digital signal to be sent is $A_m(n) = 0 (0 \leq m \leq M-1, 0 \leq n \leq N-1)$, where m indicates the data block index and n indicates the subcarrier index. After binary phase-shift keying (BPSK) modulation, $B_m(n) = 1$, which is then multiplied by the preset pseudo-random sequence to obtain $X_m(n)$ (the value is 1 or -1), then obtain $x_m(t)$ by inverse discrete Fourier transform (IDFT), and finally add the cyclic prefix (CP) as the GI. The receiver is the reverse process of the transmitter. The received signal is forwarded to the discrete Fourier transform (DFT), reverse pseudo-random, and BPSK demodulation operations to obtain $D_m(n)$.

The frame structure is shown in Fig. 3(b), the length of the data block is set to T, and the length of the CP set to T_{cp}. Fig. 3 shows the situation with only the direct path, in the case of precise synchronization, the start-stop time of the analysis window and the data block are entirely identical, so IBI and ICI are not caused. To simplify the discussion, we assume that the underwater acoustic channel is a simple two-path model, and the received signal can be expressed as:

$$r(t) = x(t) + \alpha x(t-\tau) + n(t) \quad (9)$$

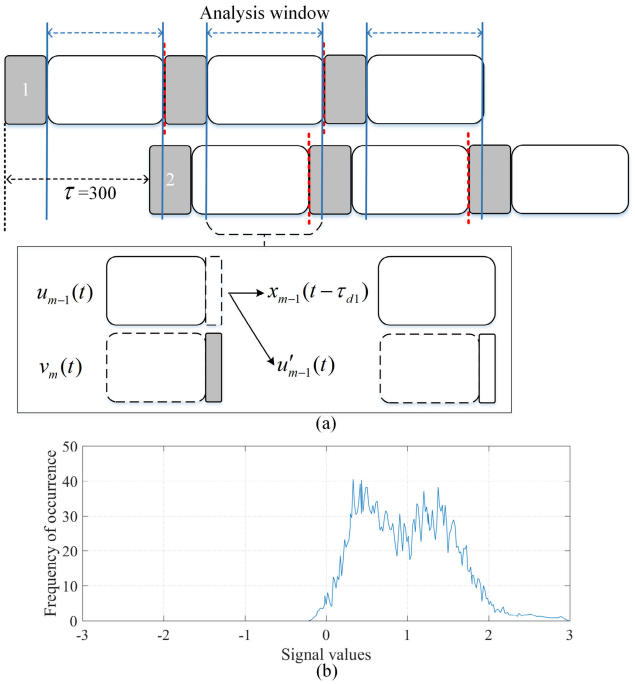

FIGURE 4. When $\tau = 300$, (a) relation between direct and delay waves; (b) received signal distribution affected by ICI.

where α and τ are the attenuation coefficient and the delay of the second path in the channel propagation, respectively. $n(t)$ is additive white Gaussian noise and is determined by the SNR. To simulate the ICI caused by multipath, we set to send 20 data blocks, with a data block length $T = 256$, a CP length $T_{cp} = 64$, a delay $\tau = 300$, and an attenuation coefficient $\alpha = 0.7$, as shown in Fig. 4(a). At the receiver, $C_m(n)$ should be equal to $B_m(n)$ when no symbol error occurs, so a symbol error occurs when the value of $C_m(n)$ is negative.

When the start-stop time of the analysis window is shown in Fig. 4(a), the time delay of the second path $\tau = 300$. The *m-1*th data block and the *m*th CP of the second path are aliased with the *m*th data block of the first path. The distribution of the real part of the received signal $C_m(n)$ is shown in Fig. 4(b), and some of these values are negative, that is, a symbol error is generated. In this simulation system, when the influence of noise is ignored, the received signal can be expressed as:

$$\begin{aligned} r_m(t) &= x_m(t) + \alpha(u_{m-1}(t) + v_m(t)) \\ &= x_m(t) + \alpha x_{m-1}(t-\tau_{d1}) \\ &\quad +\alpha(-u'_{m-1}(t) + v_m(t)) \\ u_{m-1}(t) &= \begin{cases} x_{m-1}(t-\tau_{d1}) & if\ 0 \le t \le \tau_{d1}-1 \\ 0 & if\ \tau_{d1} \le t \le N-1 \end{cases} \\ &= x_{m-1}(t-\tau_{d1}) - u'_{m-1}(t) \\ u'_{m-1}(t) &= \begin{cases} 0 & if\ 0 \le t \le \tau_{d1}-1 \\ x_{m-1}(t-\tau_{d1}) & if\ \tau_{d1} \le t \le N-1 \end{cases} \\ v_m(t) &= \begin{cases} 0 & if\ 0 \le t \le \tau_{d1}-1 \\ x_m(t-\tau_{d2}) & if\ \tau_{d1} \le t \le N-1 \end{cases} \end{aligned} \quad (10)$$

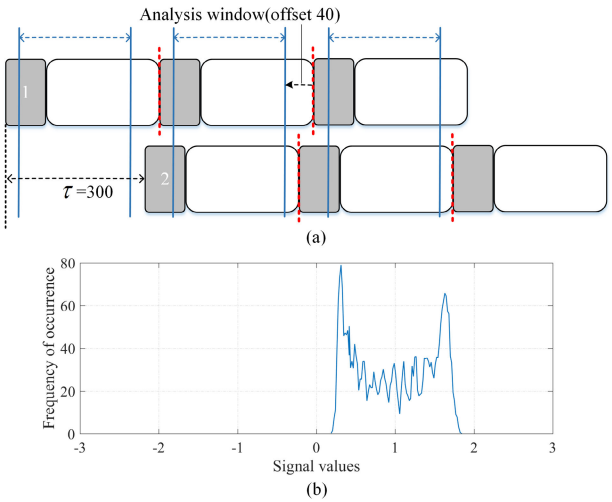

FIGURE 5. When offset = 40, (a) adjustment of analysis window; (b) received signal distribution after adjustment.

Based on the cyclic shift property, $\tau_{d1} = \tau - T_{cp}$, $\tau_{d2} = \tau_{d1} - T_{cp}$ in (10). Suppose $S_m(n)$ and $S_{m-1}(n)$ are random patterns of the *m*th and *m-1*th data blocks, respectively, consisting of 1 or -1. The real part of $C_m(n)$ can be expressed as:

$$\begin{aligned} \mathrm{Re}[C_m(n)] = 1 + \mathrm{Re}[\alpha S_m(n) S_{m-1}(n) e^{j2\pi n(\tau_{d1}/N)}] \\ +\mathrm{Re}[\alpha(-U'_{m-1}(n) + V_m(n))] \end{aligned} \quad (11)$$

In (11), $U'_{m-1}(n)$ and $V_m(n)$ are added to each subcarrier after IDFT and DFT operations in the simulation system, thereby generating ICI. ICI can be avoided by adjusting the analysis window. As shown in Fig. 5(a), we move the analysis window forward by 40 samples so that the effect of the second path on the first path is precisely in the same block. Although this displacement adjustment introduces phase rotation in the frequency domain, the phase rotation can be compensated by frequency domain equalization (FDE). The distribution of the real part of the received signal after adjusting the analysis window is shown in Fig. 5(b). All values are positive, that is, no symbol error is generated.

The above method of eliminating ICI by adjusting the analysis window requires a clear knowledge of the delay information of multipath arrival, but the exact delay of each path is usually unclear in the actual UWAC environment. We have designed a rack receiver based on the data pick, and the implementation scheme is shown in Fig. 6. Since the multipath delays $(\tau_1 \ldots \tau_i)$ and the corresponding attenuation coefficients $(\alpha_1 \ldots \alpha_i)$ are unknown, it is necessary to design multiple analysis windows for demodulation. These analysis windows are the rake fingers.

Conventional rake receivers mainly utilize multipath diversity in spread spectrum communication. In the data pick-based rake receiver scheme designed in this paper, rake reception is mainly used to find the best rake finger to minimize ICI. For these rake fingers, by examining the data errors after demodulation, and choosing the best rake finger without

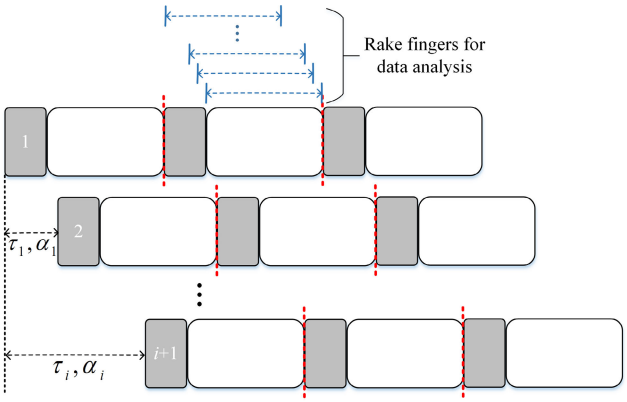

FIGURE 6. Rake fingers of data pick-based rake reception.

error, so for each data block, there is its own best rake finger. If all rake fingers have data errors, the final output data are generated by merging all decoded data in bit level.

III. ANTI-MULTIPATH OCDM SYSTEM MODEL

A. UNDERWATER ACOUSTIC CHANNEL MODELS

In this paper, two underwater acoustic channel models are used for numerical simulation. One is a dynamic underwater acoustic channel model based on Watermarkchannel [19], and the other is a static channel model constructed from the measured data in Xiamen Port.

To simulate the time-varying of the underwater acoustic channel, we consider the commonly used dynamic underwater acoustic channel simulator based on Watermarkchannel [19], which generates time-varying channel impulse response (CIR). Watermark is a freely available benchmark for physical-layer schemes for UWAC. It can easily adjust parameters to test and compare algorithms for the physical layer under realistic and reproducible conditions. Here, we use the single-input single-output (SISO) mode of the simulator. The received signal that passes through the time-varying simulation channel (called watermark time-varying channel, WMT Channel) is expressed as:

$$r(t) = \int_{-\infty}^{\infty} \hat{h}(t\,;\tau)s(t-\tau)d\tau + n(t) \tag{12}$$

where $s(t)$ is the input signal, $\hat{h}(t\,;\tau)$ is the impulse response of the time-varying channel, $n(t)$ is the noise term, and $r(t)$ is the output serial term. The continuous time-varying impulse responses are provided through a MATLAB (.mat) file for easy recall in system simulation. The WMT Channel model also considers the Doppler shift introduced by relative motion or carrier frequency offset.

In this paper, the simulation parameters for WMT Channel are as follows: the communication distance is 750 m, the water depth is 10 m, and the transducer is placed at a water depth of 8 m. Fig. 7(a) shows the normalized CIR of WMT Channel with a root mean square (RMS) channel delay spread [20] value of 9.6 ms.

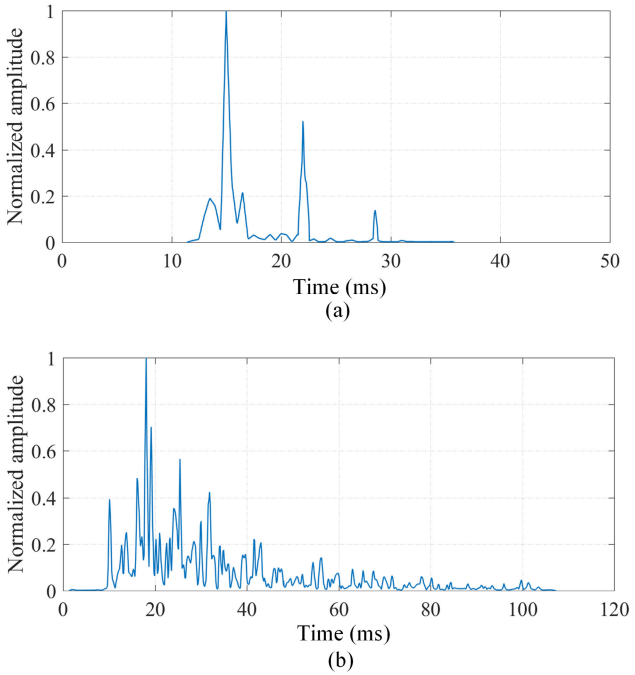

FIGURE 7. Normalized CIR for (a) WMT Channel and (b) Xiamen Port shallow water acoustic channel.

The second underwater acoustic channel model comes from the measured impulse response data of Xiamen Port Xiandai Terminal. The normalized CIR is shown in Fig. 7(b). The analysis and modeling of the underwater acoustic channel are performed using the CIR data and the BELLOP method based on Gaussian beam ray tracing, which is achieved by multiplying the attenuation coefficient at the moment of corresponding multipath delay and then adding Gaussian white noise [21]. The communication distance of Xiamen Port Xiandai Terminal is approximately 300 m, the water depth is approximately 15 m, and the transducer is placed at a water depth of 5 m. As shown in Fig. 7(b), in this shallow water, the sound transmission consists of a direct path, multiple paths that reflected by sea surface and bottom. Therefore, the Xiamen Port shallow water acoustic channel (Xiamen Port SW Channel) has severe multipath and a long delay spread, with an RMS channel delay spread value of 26 ms.

B. ANTI-MULTIPATH OCDM SCHEME

The frame structure of anti-multipath OCDM communication is shown in Fig. 8. The beginning of each frame is a preamble sequence composed of dual hyperbolic frequency modulation (HFM) signals. They can be used for accurate frame synchronization and Doppler estimation due to Doppler invariance [22]. The GI (generally set to be longer than the delay spread of the channel) is followed by a known pilot symbol for channel estimation. After the pilot symbol, the transmitted data blocks have cyclic prefixes inserted between adjacent data blocks.

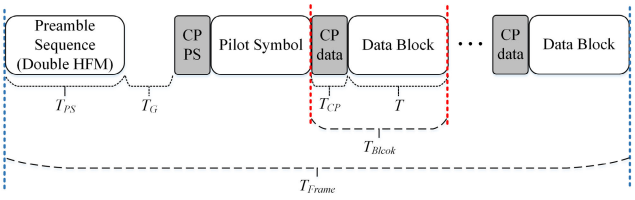

FIGURE 8. OCDM frame structure.

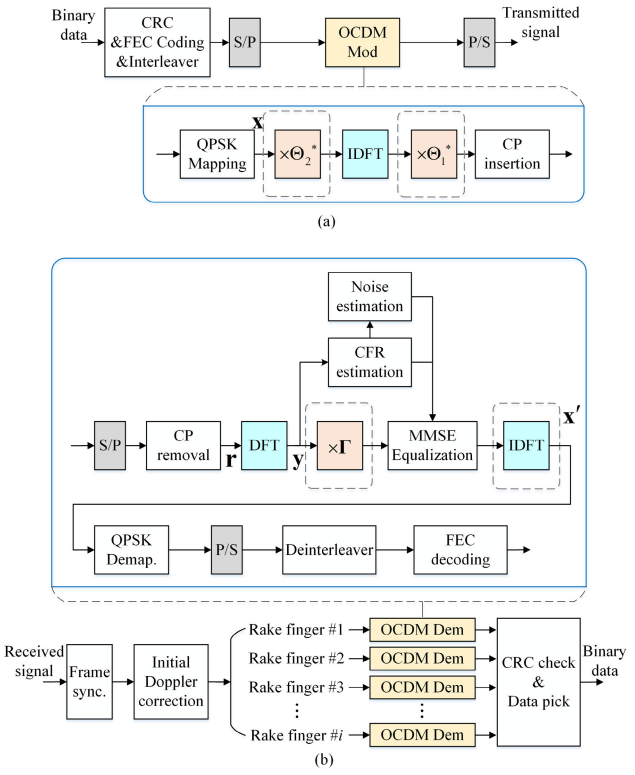

FIGURE 9. Schematic diagram of the DP-Rake OCDM system. (a) Transmitter and (b) receiver.

This section introduces a new transmission and reception scheme in the anti-multipath OCDM communication system. It combines the OCDM modulation and demodulation described in Section II.A with the data pick-based rake receiver described in Section II.B. The new system is called the data pick rake OCDM (DP-Rake OCDM). In the OCDM system, the operational process of IDFnT and DFnT should be respectively performed at the transmitter and the receiver. To be compatible with the prevalent OFDM communication system, a compatible OCDM scheme based on OFDM communication architecture is proposed in [15], this scheme only has the operation process of IDFT and DFT at the transceiver or receiver. This paper is also based on the OCDM scheme proposed in [15].

As shown in Fig. 9(a), in order to ensure the reliability of the high-rate communication system in underwater acoustic channel, the digital signal at the transmitter undergoes the following preprocessing operation: First, insert the cyclic redundancy check (CRC) codes before forward error correction (FEC) coding; the CRC overhead is typically very small, usually 16 bits (CRC-16). Then, after the CRC coding, a convolutional code is used for FEC coding that considers the balance of complexity and error correction performance; the convolutional coding parameter is set as follows: the code rate is 1/2, using the optimal generator polynomial [753, 516], the constraint length is $L = 9$, and the backtrack length is $5L$. Finally, interleaves the binary data by matrix interleaving in one frame. The preprocessed digital signal is mapped to a complex signal via QPSK, which is then modulated by OCDM and sent out. The IDFnT in OCDM modulation can be replaced by IDFT and two phase multiplications Θ_1^* and Θ_2^*, where Θ_1 and Θ_2 are diagonal matrices whose diagonal entries are $\Theta_1(m)$ and $\Theta_2(n)$, respectively. $\Theta_1(m)$ and $\Theta_2(n)$ can be expressed as:

$$\Theta_1(m) = e^{-j\frac{\pi}{4}} \times \begin{cases} e^{j\frac{\pi}{N}m^2} & N \equiv 0(\mathrm{mod}2) \\ e^{j\frac{\pi}{4N}} e^{j\frac{\pi}{N}(m^2+m)} & N \equiv 1(\mathrm{mod}2) \end{cases}$$
$$\Theta_2(n) = \begin{cases} e^{j\frac{\pi}{N}n^2} & N \equiv 0(\mathrm{mod}2) \\ e^{j\frac{\pi}{N}(n^2-n)} & N \equiv 1(\mathrm{mod}2) \end{cases} \quad (13)$$

The receiver scheme of the DP-Rake OCDM system is shown in Fig. 9(b): at first, after conversion to the baseband signal, the received signal is cross-correlated with the local dual HFM signal, the correlation peak is determined to complete the frame synchronization [22], and the Doppler shift caused by relative motion is compensated by Doppler estimation and phase correction; then, the obtained data are transferred to the data pick-based rake receiver, and each data block is subjected to OCDM demodulation under the setting of each rake finger; finally, the demodulated data is subjected to CRC check and data pick to obtain the final information data. The OCDM demodulation part adopts a single-tap FDE for the demodulation structure in [15]. The data block to be demodulated is $\mathbf{r}$, and DFT processing for $\mathbf{r}$ can obtain $\mathbf{y}$ before FDE. $\mathbf{y}$ can be expressed as:

$$\mathbf{y} = \mathbf{F}\mathbf{r} = \mathbf{\Gamma}^H \mathbf{F} \Lambda \mathbf{x} + \mathbf{w} \quad (14)$$

where $\mathbf{F}$ is the Fourier matrix of size N, $\mathbf{\Gamma}$ and $\mathbf{\Lambda}$ are both diagonal matrices of size N, which can be expressed as:

$$\{\mathbf{\Gamma}\}_{k,k} = e^{-j\frac{\pi}{N}k^2}$$
$$\{\mathbf{\Lambda}\}_{k,k} = H_k \quad (15)$$

In (14), $\mathbf{w}$ is the Gaussian noise component with a mean of 0, and the variances of $\mathbf{w}$ and $\mathbf{x}$ are σ_w^2 and σ_x^2, respectively. In (15), H_k is the channel frequency response (CFR) of the channel at the kth frequency bin.

Assume that the CFR is unchanged in one frame; after performing phase multiplication, CFR compensation and IDFT processing on $\mathbf{y}$, the symbol $\mathbf{x}'$ estimate can be obtained. This process can be expressed as:

$$\mathbf{x}' = \mathbf{F}^H \mathbf{G} \mathbf{\Gamma} \mathbf{y} \quad (16)$$

where $\mathbf{G}$ is the diagonal equalization matrix under the minimum mean square error (MMSE) criterion, which is obtained

by pilot estimation and can be expressed as:

$$\mathbf{G} = \mathbf{\Lambda}^H(\mathbf{\Lambda}^H\mathbf{\Lambda} + \frac{\sigma_w^2}{\sigma_x^2}\mathbf{I})^{-1} \tag{17}$$

The scheme of transmission and reception in the DP-Rake OCDM system as shown in Fig. 9 is perfectly compatible with the scheme of the OFDM system, wherein the dashed boxes indicate the steps added to the OFDM system: two phase multiplications at the transmitter, one phase multiplication, and one IDFT at the receiver. When considering the algorithm complexity of OCDM compared to OFDM, at the transmitter, there are only 2 additional phase multiplications per symbol. At the receiver, besides the equalizer, the additional IDFT brings an additional complexity of 0.5 $\log_2 N$ per symbol. It can be seen that the complexity of the OCDM system is slightly increased compared to that of the OFDM system, with $2 + 0.5 \log_2 N$ multiplications per symbol. In practical applications, the DP-Rake OCDM system can be implemented by upgrading the original OFDM system. At the receiver, OCDM demodulation is embedded into the data pick-based rake receiver. Multiple rake fingers can significantly increase the computational complexity of the receiver. However, the bandwidth used in UWAC is much smaller than radio frequency (RF) communication, and the amount of calculation is not a problem for current hardware resources (such as CPUs, FPGAs, etc.).

IV. SYSTEM SIMULATION RESULTS AND DISCUSSION

A. SYSTEM SIMULATION PARAMETERS

In this section, the performance of the OFDM system, OCDM system, and DP-Rake OCDM system are simulated and discussed. The simulation environment is the WMT Channel and the Xiamen Port SW Channel introduced in Section III.A. The performance metrics are the bit error rate (*BER*) and the effective data rate (*EDR*) of the demodulated binary data. The *EDR* can be defined as:

$$\begin{aligned} EDR &= (1 - PER) \cdot DR \\ DR &= \frac{N_d}{(1 + N_d)(1 + R_{CP})} BR_C \log_2 M \end{aligned} \tag{18}$$

In (18), *PER* is the packet error ratio (*PER*), which indicates the error rate of all transmitted data frames. *DR* indicates the data transmission rate.

The settings of the system simulation parameters are summarized in Table 1. For a fair comparison performance, the OFDM system, OCDM system, and DP-Rake OCDM system are consistent in the setting of simulation parameters.

B. THE WMT CHANNEL

This section uses the WMT Channel as the simulation channel. WMT Channel is a time-varying channel, so the Doppler shift and Doppler spread will inevitably be introduced in communication, but the Doppler effect is not the focus of the simulation and can be eliminated by techniques such as Doppler estimation and phase correction.

TABLE 1. System simulation parameters.

Symbol	Signification	WMT Channel	Xiamen Port SW channel
B	Bandwidth for baseband signal	4 kHz	20 kHz
f_s	Sampling frequency	120 kHz	200 kHz
f_c	Center carrier frequency	14 kHz	50 kHz
N	Number of subcarriers	256	1024
N_d	Number of data blocks pre Frame	3	10
T_{CP}	Cyclic prefix time	16 ms	12.8 ms
T_G	Guard interval time after peramble sequence	256 ms	
	Modulation	QPSK-OCDM	
M	Constellation order	4	
	FEC	Convolutional coding & Viterbi decoding	
R_C	FEC rate	1/2	
R_{CP}	Cyclic prefix ratio	1/4	
	Number of rake fingers	64	
	Number of evaluated frames	100	

Single-carrier (SC) communication with iterative FDE (SC-FDE) is a common method for underwater acoustic communication [23]. An SC-FDE system usually needs to add equalization and channel coding modules to provide better communication performance while maintaining lower computational complexity. Therefore, we chose SC-FDE as the benchmark for communication performance comparison. The choice of FDE instead of time domain equalization (TDE) is considered to be consistent with other systems in comparison. The SC-FDE system uses the same frame structure as shown in Fig. 8.

The BER performance comparison of SC-FDE, OFDM, OCDM, and DP-Rake OCDM systems is shown in Fig. 10(a): the BER performance of OFDM and SC-FDE is equivalent, which is due to the use of FEC coding, Doppler estimation, and phase correction techniques in these systems, as these techniques eliminate the Doppler shift introduced by channel variations; the BER performance of OCDM is better than OFDM because OCDM provides both spreading and diversity gain through its chirp-based signal; DP-Rake OCDM has the best BER performance, but the improvement over OCDM is not significant. The reason is that the delay spread of the WMT Channel is small relative to the CP, and leading to ICI is not severe.

The EDR performance comparison is shown in Fig. 10(b). The results are similar to those in Fig. 10(a): The OCDM and DP-Rake OCDM systems provide higher EDR performance than other systems, especially at low SNR. This result is attributed to the advantages of spreading and diversity gain in OCDM. At the same communication rate, the OCDM system requires lower SNR, which provides higher system robustness.

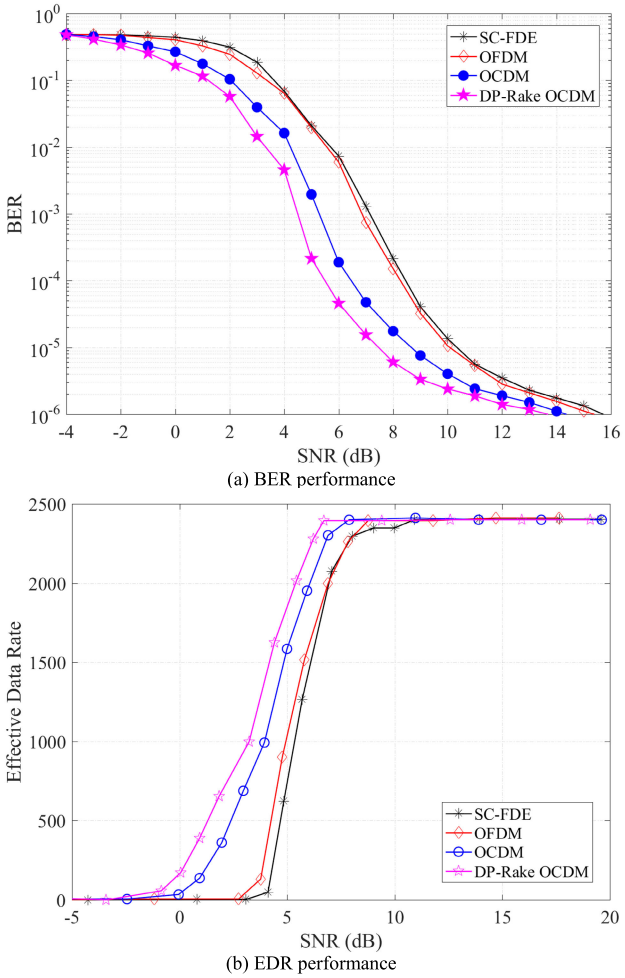

FIGURE 10. Performance comparison over the WMT channel.

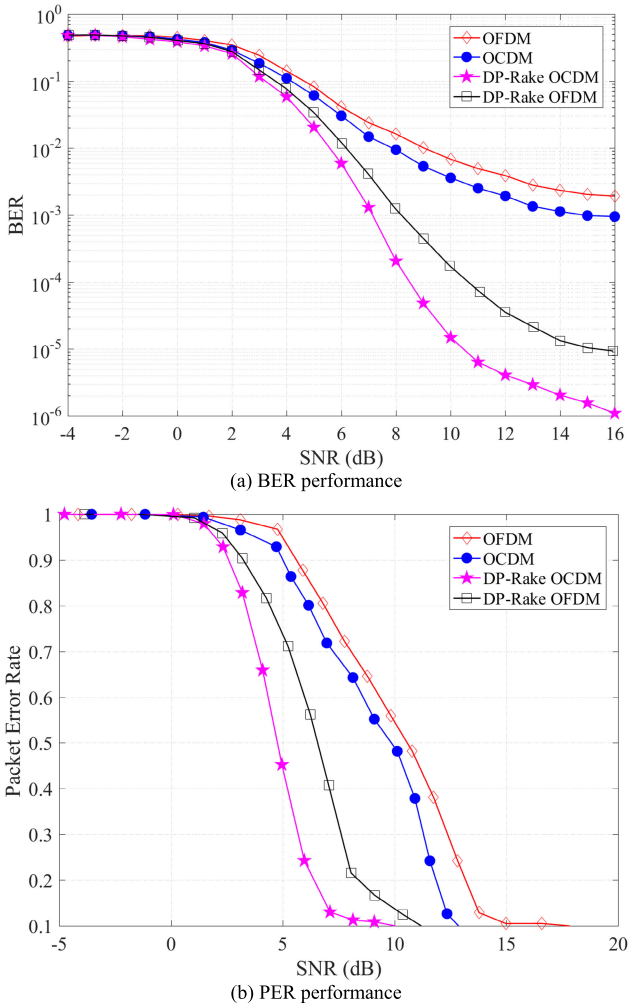

FIGURE 11. Performance comparison over the Xiamen Port SW channel.

C. THE XIAMEN PORT SW CHANNEL

This section uses the Xiamen Port SW Channel described in Section III.A as the simulation channel. The channel has a sizeable multipath delay spread, which inevitably introduces ICI into the multi-carrier communication system, thereby destroying the orthogonality of the sub-carriers and affecting communication performance. Fig. 11(a) compares the BER performance of OFDM, OCDM, Data Pick-Rake OFDM (DP-Rake OFDM) and DP-Rake OCDM multi-carrier systems, as seen in the figure: OCDM BER performance is slightly better than OFDM, but the BER performance of OFDM and OCDM are not very good, and the BER floor is approximately 10^{-3}, as the ICI introduced by delay spread has a significant influence on multi-carrier communication; the BER performance of the DP-Rake OCDM system is significantly improved because the data pick-based rake receiver, as described in Section II.B, is added to the system, which effectively eliminates ICI and breaks the BER floor of 10^{-3}. The performance of DP-Rake OFDM is between those of OCDM and DP-Rake OCDM. The additional data pick-based rake receiver enhances the performance of OFDM with a BER floor of 10^{-5}. Fig. 11(b) shows the PER performance comparison trend is the same as the BER, and the PER performance curves of OFDM and OCDM are relatively flat because the performance is affected by ICI in addition to the SNR; the DP-Rake OCDM eliminates ICI and makes SNR the main factor. Therefore, the performance curve of the DP-Rake OCDM is steeper. The simulation results verify the effectiveness of the DP-Rake OCDM for anti-multipath performance.

V. CONCLUSION

This paper proposes a new anti-multipath OCDM method to provide high robustness in severe multipath UWAC. The method is based on the Fresnel transform and uses chirp signals to utilize the diversity gain of the multipath. The transmitter and receiver structure of the OCDM system can be compatible with the conventional OFDM system by adding phase multiplications. Based on the analysis that severe multipath will introduce IBI and ICI, this paper points out that ICI can be eliminated by adjusting the analysis window. We further propose a data pick-based rack receiver with multiple rake fingers to effectively eliminate ICI and increase the data

rate at short guard intervals. We combine the principle of OCDM and the data pick-based rake receiver to form the scheme of the DP-Rake OCDM system. This paper simulates the communication performance of the OFDM, OCDM, and DP-Rake OCDM systems under two channel conditions. The performance simulation results of BER, EDR, and PER show that OCDM performance is better than that of OFDM, but it is greatly affected by ICI. DP-Rake OCDM can effectively eliminate the ICI caused by multipath delay spread and improve communication performance. Therefore, DP-Rake OCDM has great value in the shallow water acoustic channel with severe multipath. In future work, we will consider the impact of the Doppler effect on the DP-Rake OCDM system and the corresponding improvement methods.

ACKNOWLEDGMENT

The authors would like to thank Dr. Xiaokang Zhang from the College of Ocean and Earth Science, Xiamen University, for providing the measured impulse response data of Xiamen Port Xiandai Terminal. They would also like thank Hui Wu and American Journal Experts (AJE) for language editing, which has improved the manuscript.

REFERENCES

[1] M. Chitre, S. Shahabudeen, and M. Stojanovic, "Underwater acoustic communications and networking: Recent advances and future challenges," *Mar. Technol. Soc. J.*, vol. 42, no. 1, pp. 103–116, Mar. 2008.

[2] C. Lal, R. Petroccia, M. Conti, and J. Alves, "Secure underwater acoustic networks: Current and future research directions," in *Proc. IEEE 3rd Underwater Commun. Netw. Conf. (UComms)*, Lerici, Italy, Aug. 2016, pp. 1–5.

[3] T. C. Yang, "Properties of underwater acoustic communication channels in shallow water," *J. Acoust. Soc. Amer.*, vol. 131, no. 1, pp. 129–145, Jan. 2012.

[4] E. Baktash, M. J. Dehghani, M. R. F. Nasab, and M. Karimi, "Shallow water acoustic channel modeling based on analytical second order statistics for moving transmitter/receiver," *IEEE Trans. Signal Process.*, vol. 63, no. 10, pp. 2533–2545, May 2015.

[5] B. Reynders and S. Pollin, "Chirp spread spectrum as a modulation technique for long range communication," in *Proc. Symp. Commun. Veh. Technol. (SCVT)*, Mons, Belgium, Nov. 2016, pp. 1–5.

[6] L. Marchetti and R. Reggiannini, "An efficient receiver structure for sweep-spread-carrier underwater acoustic links," *IEEE J. Ocean. Eng.*, vol. 41, no. 2, pp. 440–449, Apr. 2016.

[7] H. Ochi, T. Tsuchiya, Y. Amitani, M. Suzuki, and S. Negishi, "Study on color video pictures transmission by digital acoustic signal," in *Proc. Conf. Pacific Ocean Environ. Probing*, Okinawa, Japan, Aug. 1992, pp. 132–137.

[8] M. Stojanovic, J. Catipovic, and J. Proakis, "Phase coherent digital communications for underwater acoustic channels," *IEEE J. Ocean. Eng.*, vol. 19, no. 1, pp. 100–111, Jan. 1994.

[9] T. Eggen, A. Baggeroer, and J. Preisig, "Communication over Doppler spread channels. Part I: Channel and receiver presentation," *IEEE J. Ocean. Eng.*, vol. 25, no. 1, pp. 62–71, Jan. 2000.

[10] T. Eggen, J. Preisig, and A. Baggeroer, "Communication over Doppler spread channels. II. Receiver characterization and practical results," *IEEE J. Ocean. Eng.*, vol. 26, no. 4, pp. 612–621, 2001., Oct. 2001.

[11] M. Stojanovic, "Low complexity OFDM detector for underwater acoustic channels," in *Proc. OCEANS*, Boston, MA, USA, Sep. 2006, pp. 1–6.

[12] F. Qu and L. Yang, "Basis expansion model for underwater acoustic channels?" in *Proc. OCEANS*, Quebec City, QC, Canada, Sep. 2008, pp. 1–7.

[13] X. Ouyang, O. A. Dobre, Y. L. Guan, and J. Zhao, "Chirp spread spectrum toward the Nyquist signaling rate–orthogonality condition and applications," *IEEE Signal Process. Lett.*, vol. 24, no. 10, pp. 1488–1492, Oct. 2017.

[14] Y. Bai and P.-J. Bouvet, "Orthogonal chirp division multiplexing for underwater acoustic communication," *Sensors*, vol. 18, no. 11, p. 3815, Nov. 2018.

[15] X. Ouyang and J. Zhao, "Orthogonal chirp division multiplexing for coherent optical fiber communications," *J. Lightw. Technol.*, vol. 34, no. 18, pp. 4376–4386, Sep. 15, 2016.

[16] C. R. Berger, J. P. Gomes, and J. M. F. Moura, "Sea-trial results for cyclic-prefix OFDM with long symbol duration," in *Proc. MTS/IEEE OCEANS Conf.*, Santander, Spain, Jun. 2011, pp. 1–8.

[17] H. Talbot, "LXXVI. Facts relating to optical science. No. IV," *Philos. Mag. J. Sci.*, vol. 9, no. 56, pp. 401–407, Dec. 1836.

[18] B. Sharif, J. Neasham, O. Hinton, and A. Adams, "A computationally efficient Doppler compensation system for underwater acoustic communications," *IEEE J. Ocean. Eng.*, vol. 25, no. 1, pp. 52–61, Jan. 2000.

[19] P. A. Van Walree, F.-X. Socheleau, R. Otnes, and T. Jenserud, "The watermark benchmark for underwater acoustic modulation schemes," *IEEE J. Ocean. Eng.*, vol. 42, no. 4, pp. 1007–1018, Oct. 2017.

[20] J. G. Proakis, and M. Salehi, "Fading channels I: Characterization and signaling," in *Digital Communications*, 5th ed. Boston, MA, USA: McGraw-Hill, 2008, pp. 830–891.

[21] W. Q. Yang and X. M. Xu, "Comparison of performances of turbo codes with different modulation methods in underwater acoustic communication," *Suppl. Tech. Acoust.*, vol. 1, no. 2, pp. 101–102, Feb. 2006.

[22] P. B. Zhu, X. M. Xu, and Y. Tao, "Research on network node technology of underwater acoustic communication based on LabVIEW," *J. Xiamen Univ.*, vol. 03, no. 4, pp. 364–367, May 2010.

[23] Y. R. Zheng, J. Wu, and C. Xiao, "Turbo equalization for single-carrier underwater acoustic communications," *IEEE Commun. Mag.*, vol. 53, no. 11, pp. 79–87, Nov. 2015.

PEIBIN ZHU received the B.S. and M.S. degrees from the College of Ocean and Earth Science, Xiamen University, China, in 2010, where he is currently pursuing the Ph.D. degree. From 2010 to 2016, he was a Research and Development Engineer with JX Instrument Company, Ltd., Shanghai, where he was responsible for the development of embedded test and measurement systems. His research interests include underwater acoustic signal processing, underwater acoustic communication, and networks.

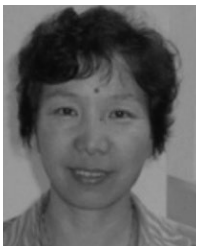

XIAOMEI XU received the M.S. degree in underwater acoustic telemetry and the Ph.D. degree in underwater communications from Xiamen University (XMU), China, in 1988 and 2002, respectively. In 1994 and 1995, she was with Oregon State University, OR, USA. She is currently a Professor with the College of Ocean and Earth Science, XMU. Her research interests include underwater communication, underwater acoustic telemetry, and underwater acoustic networks.

XINGBIN TU received the B.S. degree from the College of Ocean and Earth Science, Xiamen University, China, in 2012, and the master's degree Xiamen University, where he is currently pursuing the Ph.D. degree. From 2016 to 2018, he was a Visiting Scholar with The University of Alabama, AL, USA. His research interests include underwater acoustic communications and signal processing.

YOUGAN CHEN (Senior Member, IEEE) received the B.S. degree from Northwestern Polytechnical University (NPU), Xi'an, China, in 2007, and the Ph.D. degree from Xiamen University (XMU), Xiamen, China, in 2012, all in communication engineering.

He visited the Department of Electrical and Computer Engineering, University of Connecticut (UCONN), Storrs, CT, USA, from November 2010 to November 2012. He has been an Assistant Professor with the Department of Applied Marine Physics and Engineering, XMU, since 2013. He has authored or coauthored more than 50 peer-reviewed journal/conference papers. He holds 12 China patents. He is the PI of seven national/provincial natural science foundation projects and the Co-PI of six more projects. His research interests include the areas of communications and signal processing, currently focusing on channel coding and cooperative communications for underwater acoustic channels.

Dr. Chen has served as a TPC Member of the IEEE ICSPCC 2019. He has served as a Secretary of the IEEE ICSPCC 2017. He has received the Technological Invention Award of Fujian Province, China, in 2017. He has been served as an Associate Editor for IEEE Access, since 2019. He has served as the Technical Reviewer for many journals such as the IEEE Journal of Oceanic Engineering, the IEEE Transactions on Communications, IEEE Access, *Sensors*, and *IET Communications*. He has served as the Technical Reviewer for conferences such as ACM WUWNet.

YI TAO (Member, IEEE) was born in Chongqing, China, in 1973. He received the B.S. degree in computer science and applications from Hangzhou Dianzi University, China, in 1998, the M.S. degree in computational fluid mechanics (SIAMM) from Shanghai University, China, in 2003, and the Ph.D. degree in marine sciences from Xiamen University (XMU), China, in 2008.

Since 2008, he has been an Assistant Professor with the Department of Applied Marine Physics and Engineering, XMU. His research interests include marine acoustic signal processing and underwater acoustic communication.